# Origin of High Friction at Graphene Step Edges on Graphite

Zhe Chen, Arash Khajeh, Ashlie Martini, and Seong H. Kim<sup>1,\*</sup>

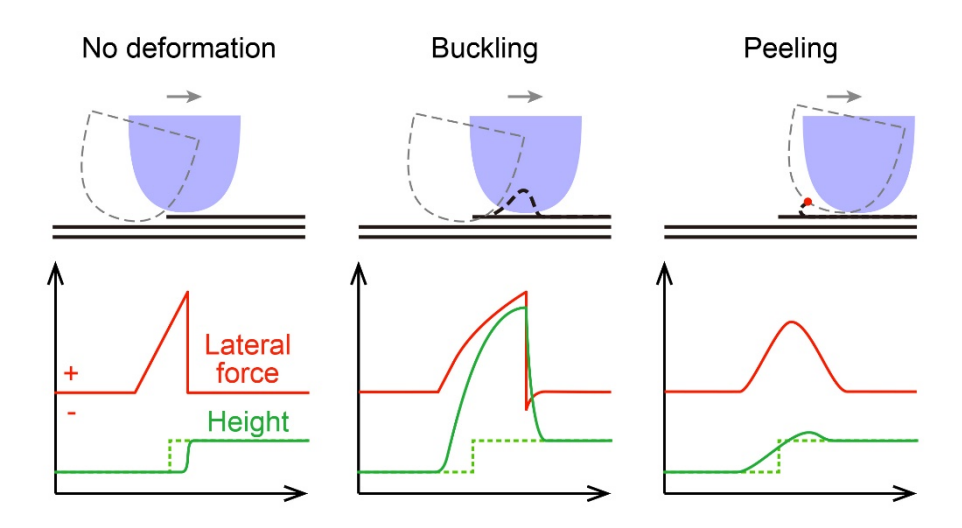
- <sup>1</sup> Department of Chemical Engineering and Materials Research Institute, Pennsylvania State University, University Park, PA 16802, USA.
- <sup>2</sup> Department of Mechanical Engineering, University of California Merced, Merced, CA 95343, USA.
- \* Corresponding authors: amartini@ucmerced.edu and shkim@engr.psu.edu

## **ABSTRACT**

On graphite, friction is known to be more than an order of magnitude larger at step edge defects as compared to on the basal plane, especially when the counter surface slides from the lower terrace of the step to the upper terrace. For this observation, very different mechanisms have been proposed to explain this phenomenon, including atomic interactions between the counter surface and step edge (without physical deformation) and buckling or peeling deformation of the upper graphene terrace. Here, we use atomic force microscopy (AFM) and reactive molecular dynamics (MD) simulations to capture and differentiate the mechanisms proposed to cause high friction at step edges. AFM experiments reveal the difference between cases of no deformation and buckling deformation, and the latter case is attributed to the physical stress exerted by the sliding tip. Reactive MD simulations explore the process of peeling deformation due to tribochemical bond formation between the tip and the step edge. Combining the results of AFM experiments and MD simulations, it is found that each mechanism has identifiable, characteristic

features in the lateral force and vertical height profiles recorded during the step-up process. The results demonstrate that buckling and peeling deformation of the graphene edge rarely occur under typical AFM experimental conditions, and thus are unlikely to be the origin of high friction at step edges in most measurements. Instead, the high step-up friction is due to stick-slip behavior facilitated by the topographical change and atomic interactions between the tip and step edge without deformation of the graphene itself.

**Table of Contents Graphic** 



# Keywords

Graphene step edge; buckling; peeling; atomic force microscopy; reactive molecular dynamics simulation

#### 1 Introduction

Friction at sliding solid-solid contacts is significantly influenced by the way the material in and around the contacting region responds to shear. For graphite and graphene, most studies have focused on the super-lubricious basal plane region and shown that shear-induced basal plane deformation (often referred as to puckering) can increase friction by one or two times. However, even higher friction arises at step edge defects where one graphene layer starts or ends. It was reported that the friction at step edges can be 20 to 60 times higher than that on the basal plane when sliding proceeds in the direction from a lower terrace to an upper terrace. Understanding friction at these step edges is therefore critically important to understanding friction on graphite or graphene, as well as other two-dimensional (2D) materials that necessarily exhibit step edge defects.

To explain high friction at step edges, several mechanisms have been proposed. These mechanisms can be generally categorized into two groups, depending on whether deformation of the upper graphene terrace occurs or not. In the absence of deformation, as illustrated in Figure 1a, resistance to sliding is attributable to the topographic height change at the step and to atomic or chemical interactions between the tip and the step edge. The topography change results in a resistive force when the tip ascends the step and an assistive force as it descends the step. In contrast, atomic or chemical interactions always lead to resistive force regardless of sliding direction. Early work explained the effect of atomic interactions using a Lennard-Jones potential, and attributed the high friction at the step edge to a high potential barrier on the upper terrace side and a deep potential well on the lower terrace side of the step edge. 11-12 Then, our previous study showed that dangling bonds at step edges on graphene generated through mechanical exfoliation will be passivated with water molecules impinging from the gas phase, forming C-OH groups that

form hydrogen bonds with the oxide layer of the counter surface, leading to a resistive force.<sup>6-7</sup> Later, it was discovered that conformational changes of functional groups at the step edge, without deformation of the upper terrace, can also contribute to resistive force during the step-up process.<sup>13</sup>

The second group of mechanisms involves deformation of the upper graphene terrace. Within this group, two possible modes have been proposed, buckling and peeling. 14-19 In the case of buckling, the step is pushed up while the sliding tip is still on the lower terrace resulting in convex deformation of the upper terrace (Figure 1b). Such topographic deformation causes high friction because the tip must slide over the deformed upper terrace. 14-18 In the case of peeling, the upper terrace end is pulled up by the tip (Figure 1c); such deformation can occur if chemical bonds are formed between the step edge and counter surface. 19 Although buckling and peeling have been demonstrated in MD simulations, 14, 16-19 these mechanisms are not directly corroborated by experimental evidence. Instead, experimental studies that propose buckling or peeling support the hypothesis based on folded or ruptured graphene step edges imaged after sliding. 8, 19 However, such post-test analyses cannot determine if the mechanism was buckling, peeling, folding, or some other type of deformation.

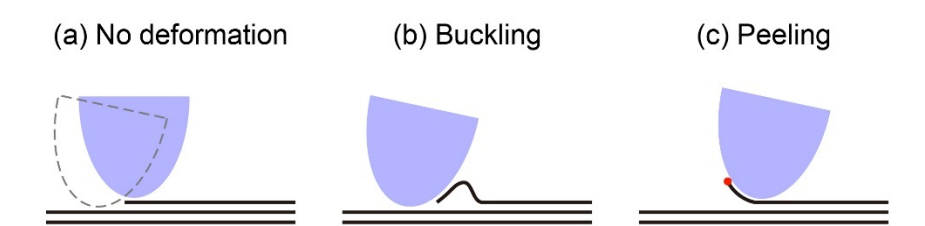


**Figure 1.** Illustration of different mechanisms proposed to cause the high friction at graphene step edges. (a) The upper terrace graphene layer does not deform due to interfacial shear. Or, deformation occurs and is the origin of the high friction, where the deformation can be (b) buckling or (c) peeling. The red dot in (c) indicates chemical bonds between the tip and the graphene edge.

In this paper, we further investigate the mechanisms for high friction at a single layer graphene step edge on a graphite surface. Although various mechanisms have been proposed in previous papers, no study directly compared all three possible cases illustrated in Figure 1, so the dominant mechanism has not been unambiguously identified. The scope of this study is limited to the case where high friction is observed during the ascending of the step without causing permanent deformation or damage to the step. Lateral force and height of the tip are monitored simultaneously in atomic force microscopy (AFM) experiments and reactive molecular dynamics (MD) simulations. The relationship between lateral force and height is found to be different for the different possible mechanisms, so these measurements can be used as a signature to identify the origins of high friction at graphene step edges. The observation-mechanism correlations shown in this study of graphene are likely extensible to other 2D materials as well.

# 2 Materials and methods

# **Experimental**

All measurements were performed with a commercial AFM system (Multimode, Bruker, US), operating in ambient environment. We used several Si AFM probes (ESP-V2, Bruker, US; nominal spring constant: 0.2 N/m, nominal tip radius: 8 nm) from the same batch purchased. The normal spring constant of the AFM probe cantilever was calibrated following the Sader's method.<sup>20</sup> The lateral sensitivity of the system was calibrated by rubbing the AFM tip against a diamond-like carbon film in *n*-pentanol vapor, for which the coefficient of friction is about 0.15 and wear is negligible.<sup>21-22</sup>

For the friction test, a fresh graphite surface was prepared through tape-exfoliation of a highly-oriented pyrolytic graphite (HOPG) substrate in ambient air. The AFM tip was treated with

UV/ozone for 15 minutes to remove possible organic contaminants from the native oxide at the tip surface. Before the friction test, an exposed single-layer graphene step edge, which is nearly parallel to the AFM probe cantilever, was found on the graphite surface. The lateral force due to friction was measured while the AFM tip was sliding perpendicular to the graphene step edge and reciprocating between the lower and upper terraces at the same location. The sliding stroke across the step edge was 100 nm, the reciprocating frequency was 2.5 Hz, and thus the sliding speed was 500 nm/s. The normal load applied to the AFM tip ranged from 2 nN to 26 nN. According to the Derjaguin-Muller-Toporov contact model,<sup>23</sup> using the nominal tip radius, the contact pressure between the tip and the graphite basal plane was in the range from 1.7 to 2.7 GPa. Since the compressive strength of Si is reported to be 3.2 GPa, the upper limit of the applied normal load was kept at 26 nN (2.7 GPa) to avoid physical deformation and wear of the tip. The pull-off force of the AFM tip on the graphite basal plane were respectively measured before and after the friction test, and the value was kept around 7 nN (Figure S1), indicating that wear or damage of the AFM tip is negligible. Moreover, as shown in Figure S2, in multiple successive scans at the same location, the lateral force signal always begins to increase at the same lateral position, and the stepdown position does not change either, indicating that the upper terrace graphene layer remains intact.

#### MD simulations

The friction behavior of an amorphous silica tip apex sliding up a graphite step-edge was modeled using reactive MD simulations in LAMMPS code <sup>24</sup>, and OVITO software <sup>25</sup> was used to visualize the results. The ReaxFF <sup>26</sup> force field used in this work was previously developed for a C/O/H/Si/F system.<sup>27</sup> The force field parameters are a combination of parameters for C/H/O <sup>28</sup>-

<sup>29</sup> and Si/C interactions, <sup>30</sup> and were obtained by training against density functional theory (DFT) data. The ReaxFF force field is capable of modeling bond formation/breaking (chemical reactions) as well as bond stretching and bending (mechanical properties), <sup>31-32</sup> and has been used previously to investigate mechanochemical reactions.<sup>33</sup> Note that the ReaxFF force field used here was reported to overestimate the elastic modulus of pristine graphene.<sup>34</sup> Figure S3 in the Supporting Information illustrates the setup used in simulations including an amorphous hydroxylated silica tip and a graphite substrate with an exposed single-layer step edge. This model has been used in our previous studies and details are reported elsewhere.<sup>6, 13</sup> The silica surface is known to be passivated with hydroxyl groups if cleaned properly. 35-37 To mimic the passivation of the silica tip surface, the under-coordinated silicon and oxygen atoms were terminated with hydrogen atoms. In a few simulations, several H/OH groups were intentionally removed from the surface of the silica tip, and three under-coordinated silicon atoms were left on the leading edge of the tip. Since previous studies<sup>38-39</sup> reported the dissociation of water and hydroxylation at step edges, the terminal carbon atoms at the armchair step-edge<sup>40</sup> were passivated by alternating H/OH groups. In order to facilitate the deformation of the upper terrace, a nonperiodic boundary condition was used in all directions. Throughout the simulation, the bottom-most graphene layer at each side of the step edge was kept fixed, and the top 0.5 nm of the tip was treated as a rigid body; all other atoms could move freely.

Each simulation was performed in the following steps. First, the energy was minimized, followed by equilibration of the system until the potential energy reached a plateau. Next, the gap between the tip and substrate was decreased by lowering the top rigid part of the tip at a 10 m/s downward speed until the minimum distance between the tip and the substrate reached 0.3 nm. Then, a normal load of 5, 10 or 15 nN was applied to the top rigid part of the tip for 120 ps. Lastly,

the tip was dragged toward the step edge with a harmonic spring (spring constant of 6 N/m) at 10 m/s. To maintain the temperature at around 300 K, the NVT (fixed number of particles, volume, and temperature) ensemble with a Langevin thermostat was applied to the unconstrained atoms, excluding the atomic velocities in the sliding direction. A 0.25 fs time step and a 20 fs thermostat damping factor were used in all simulations. The friction force during sliding was calculated by monitoring the sum of the force on the tip atoms in the sliding direction. Throughout the simulations, the covalent bonds between atoms were identified as those with a bond order of 0.3 or larger.

### 3 Results and Discussion

Figure 2 shows the lateral force and height profiles of a Si AFM tip sliding across an exposed single-layer graphene step edge. Each line profile in this figure is the average of data collected in multiple scans (see Figure S2 in Supporting Information). During the step-up scan, a positive lateral force means resistance to the sliding motion of the AFM tip, and a negative lateral force corresponds to assistance to the motion. During the step-down scan, the sign of the lateral force has the opposite meaning, *i.e.*, negative is resistive and positive is assistive. It should be noted that, in an AFM system, the magnitude of the lateral force (or lateral signal) reflects the degree of tilting of the AFM tip or the twisting of the AFM probe cantilever, and the recorded lateral position shows the relative position between the AFM probe cantilever and the sample stage.

The deformation-free mechanism illustrated in Figure 1a is observed at low load conditions as shown in Figure 2a. In this case, the recorded height is close to a step function with height equal to the thickness of a single-layer graphene (0.34 nm). Likewise, the lateral force exhibits typical stick-slip behavior where the force initially increases linearly as the recorded lateral position of

the tip passes over the step edge and then drops back to the original value (which is the lateral force on the basal plane). The height profile shows that the tip "sticks" on the lower terrace while the lateral force is increasing, and then "slips" to the upper terrace when the lateral force drops. A dashed line parallel to the linearly increasing part of the lateral force signal is drawn in Figure 2a. The slope of this dashed line is the torsional spring constant (in nN/nm) of the AFM probe, which is the lateral sensitivity of the position sensitive detector (PSD) of the AFM system (in mV/nm) multiplied by the lateral force conversion factor of the AFM probe (in nN/mV). The lateral sensitivity and the conversion factor will not change as long as the AFM beam alignment is not changed substantially and the tip height does not decrease due to severe wear of the tip. 41 In our previous work, stick-slip behavior was observed at exposed step edges with another AFM Si probe. 13 The same AFM probe was also used to investigate the friction properties of a buried step edge. It was found that the buried step edge has exactly the same topographic dimensions as the exposed step edge, but does not result in stick-slip behavior.<sup>13</sup> The main difference between the buried and exposed step edges is that the exposed step edge contains hydroxyl groups and thus is capable of forming transient hydrogen bonds with the AFM tip while the buried step edge is completely chemically inert. Therefore, it is believed that the magnitude of the maximum lateral force before the onset of slip is due to not only the topography at the step edge, but also chemical interactions between the step edge and the tip. This also explains why the tip apex is not stuck at the step edge and the lateral force does not show stick-slip behavior as the tip descends an exposed step edge.

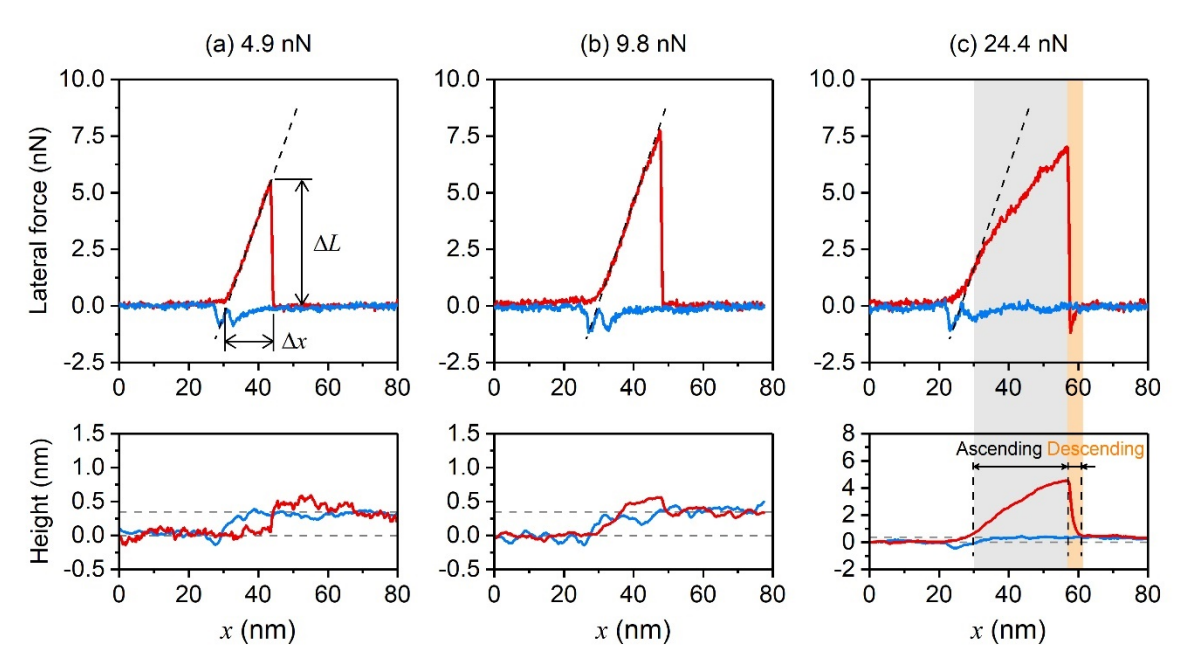


**Figure 2.** Lateral force and height profiles of an AFM tip as it slides across an exposed step edge at applied normal loads of (a) 4.9 nN, (b) 9.8 nN, and (c) 24.4 nN. The data collected during step-up are shown in red and the data during step-down are in blue. The height is set to zero when the tip is on the lower terrace. In the height profile, the dotted horizontal lines show the vertical positions of the lower and upper terraces. Note that the scale of the height profile in (c) is different from those in (a) and (b). The dashed line on the lateral force plot in (a) corresponds to linear fit of the increase of lateral force when the tip reaches and sticks at the step edge. Dashed lines in (b) and (c) have the same slope with the dashed line in (a). The gray shaded region in (c) identifies the nonlinear increase of lateral force with cantilever position, indicating step deformation. The orange shaded region indicates the gradual decrease of the tip height after the tip slips over the vertex of the buckled part of the upper terrace.

At the intermediate load (Figure 2b), as the tip slides across the step edge, the height increases gradually rather than abruptly, and there seems to be an overshoot slightly higher than the thickness of a single graphene layer. However, the magnitude of the height overshoot is small and comparable to the thermal noise of the AFM system in our experimental conditions. Therefore, it is difficult to interpret the height data with confidence. Nevertheless, the lateral force at the intermediate load again exhibits stick-slip behavior at the step edge, and the increasing part of the

lateral force is nearly parallel to the dashed line. Therefore, it is believed that physical deformation of the upper terrace is still negligible.

In contrast, at a higher load (Figure 2c), the increasing lateral force at the step edge can be divided into two parts. Firstly, the lateral force increases linearly and the slope is almost the same as the torsional spring constant of the AFM probe (indicated by the dashed line in Figure 2c), indicating that the apex of the tip does not move and the step edge is not deformed. In the second part (indicated by the gray shaded region in Figure 2c), the lateral force is still increasing, but the slope of the lateral force profile is smaller than that of the dashed line. This smaller slope means that the apex of the AFM tip is sliding from its original stuck position along the scan direction, but the tip still cannot slide freely as it does on the super-lubricous basal plane. Notably, the recorded height is significantly above the upper terrace when the recorded lateral force is below the straight dashed line. This means that the upper terrace of the step edge severely buckles (as illustrated in Figure 1b) and the tip is sliding over the buckled region. The onset of the lateral force decrease coincides with the decrease in the height profile. For the severe buckling case (Figure 2c), as the tip passes over the vertex and is descending the buckled region, the tip experiences a force assisting motion, so the recorded lateral signal becomes negative. Note that the descending distance (highlighted by the light orange shaded region in Figure 2c) is much shorter than the ascending distance (highlighted by the light grey shaded region in Figure 2c). This is because the buckled graphene layer elastically recovers once the tip passes over the vertex of the buckled upper terrace. This elastic recovery is confirmed by the data from the step-down scans (blue in Figure 2), where the lateral force remains ultralow, indicating that upper terrace is atomically flat. This is further corroborated by the observation that the onset of the lateral force increase in subsequent step-up scans occurs at the same horizonal position as in the previous scan (Figure S2).

Based on the data in Figure 2, one may speculate that buckling deformation is more likely to occur at higher applied normal loads, and that there will be a transition from no-deformation (illustrated in Figure 1a) to elastic buckling (illustrated in Figure 1b) as the normal load increases. To confirm this idea, five AFM probes (all from the same batch purchased from one vendor) were used to repeat the sliding test at various normal loads. The width (labeled  $\Delta x$  in Figure 2a) and maximum lateral force (labeled  $\Delta L$  in Figure 2a) of the stick-slip pattern at the step measured from the five sets of tests are plotted in Figure 3. The width ( $\Delta x$ ) is the distance the AFM probe moves while the tip apex is stuck at the step edge.

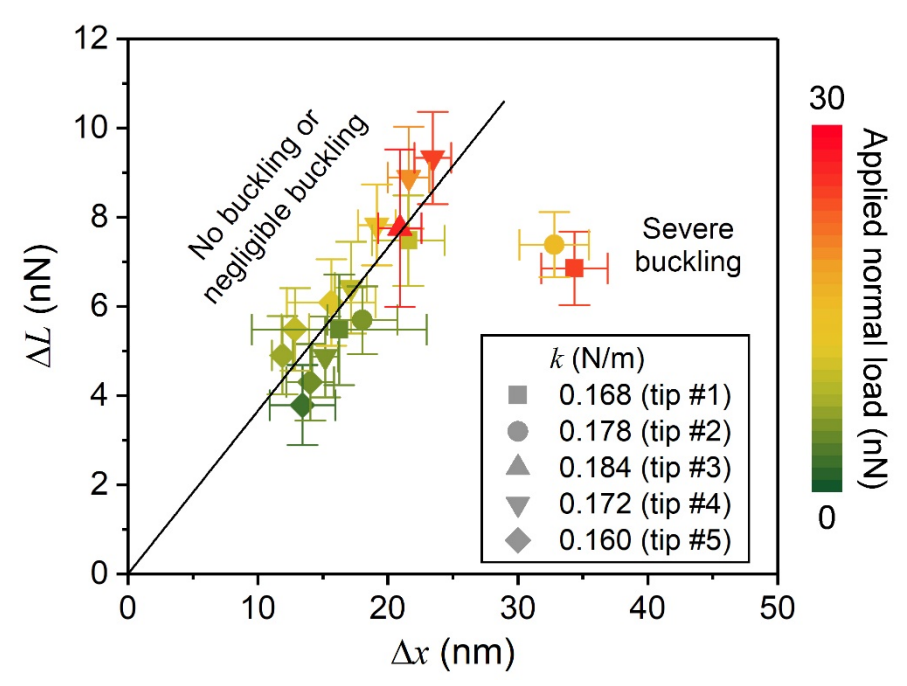


**Figure 3.** Width  $(\Delta x)$  and maximum lateral force  $(\Delta L)$  of the stick-slip behavior of multiple AFM probes at various applied normal loads. The data collected through at least 64 successive scans at each applied normal load are represented by one symbol. The error bars reflect the standard deviation of the data measured in different scans. Each symbol shape represents one AFM probe. The color of the symbols indicates the applied normal load as defined in the color bar. All AFM probes used in this experiment were from the same batch purchased and so should have similar cantilever size and tip geometry.

In Figure 3, most data falls on a single trend line. The ratio  $\Delta L/\Delta x$  is effectively the average torsional spring constant of the five AFM probes. Since all these AFM probes were from the same batch, they should have similar tip geometry and cantilever dimensions. Moreover, their measured vertical spring constants (see the legend of Figure 3) are similar. Thus, it is reasonable to expect the torsional spring constants for the different probes to be similar to each other. This is consistent with the observation that the data collected from different AFM probes can be fitted with a single straight line. Therefore, all data points around the straight line represent cases of no buckling or negligible buckling (e.g. Figure 2a and 2b), and only the two points that are relatively far from the trend line correspond to severe buckling cases (e.g. Figure 2c). Given that significant buckling was never observed in our previous work with various types of AFM probes or reported by other groups, and only two out of sixteen measurements with five probes from the same batch used here show the severe buckling behavior, it can be concluded that severe buckling is quite rare compared to cases of no or negligible buckling.

Considering the load for each case in Figure 3, it can be said that a relatively high load may result in buckling, but a high load does not necessarily lead to buckling. Therefore, the deformation of the upper terrace must be affected by other factors such as the nanoscale geometry of the AFM tip apex and the local structure or chemistry of the graphene step edge. However, these factors cannot be controlled reliably (or reproducibly) in AFM experiments. So just increasing the applied normal load does not guarantee the occurrence of buckling. It is also important to note that, the maximum lateral force of the severe buckling case (Figure 2c) is not necessarily higher than that of no or negligible buckling cases (Figure 2b). This is because when buckling occurs, the AFM tip apex slides on the buckled upper terrace instead of being stuck at the original step position, and hence the AFM tip is less tilted. Therefore, neither the magnitude of the applied normal load nor

the maximum lateral force can be used to determine whether buckling deformation occurs or not. Instead, the feature that is characteristic of buckling is lateral force increasing non-linearly as the AFM probe moves forward. Nevertheless, the rareness of observing the signature of buckling (i.e., non-linear increase of the lateral force signal) also indicates that buckling of the upper terrace is unlikely to be the dominant mechanism of the high friction at the step edge under typical AFM measurement conditions.

Peeling deformation of the upper graphene layer (as illustrated in Figure 1c) has also been proposed as a cause of high friction at step edges. <sup>19</sup> Although the AFM data shown in Figures 2 and 3 can be fully described by the mechanisms of no deformation or buckling, the possibility of peeling should be tested independently to rule it out as a governing mechanism. In our experiments, we do not expect that wedge-type peeling can occur because the AFM tip is not sharp enough to go under and lift the upper terrace. However, peeling may occur when covalent bonds are formed between the step edge and the sliding counter surface. Such bonds bridging two surfaces can be formed through tribochemical reactions under interfacial shear. <sup>13, 33, 43-47</sup> Since reactive MD simulation allows precise control of reaction sites on the sliding surfaces and monitoring of chemical bond formation during the sliding process, we use reactive MD simulations to investigate the peeling deformation. Note that reproducing stick-slip behavior <sup>48</sup> is not the main focus of the reactive MD simulations; instead, it is to identify characteristic features in the friction and topography profiles associated with peeling deformation caused by shear-induced interfacial bond formation.

In our previous MD simulation using the same model system,<sup>6, 13</sup> the atoms at the perimeter of the graphite substrate were fixed to mimic a long step edge, and no buckling or peeling was observed. Here, we changed the boundary conditions by making the perimeter atoms free,

effectively modeling a thin strip of graphene. Figures 4a-4c show the results from three simulations of a silica tip ascending an exposed single-layer graphene step edge under applied normal loads of 5 nN, 10 nN, and 15 nN. In the fourth case, we intentionally create highly reactive sites in the front side of the tip to show the impact of the tribochemical bond formation (Figure 4d). During sliding, the lateral force, tip vertical position, and number of covalent bonds between the tip and the step edge are recorded as a function of tip lateral position. The lateral position tracks the mass center of the tip and it is set as zero when the mass center of the tip is above the last carbon atom of the upper terrace. The tip vertical position tracks the rigid top part of the tip and it is set to zero when the tip is on the lower terrace after initial loading. During step-up, the resistive lateral force starts to increase as the front part of the tip touches the step edge, and covalent bonds can be formed between the tip and step edge through tribochemical reactions. In Figure 4, the first covalent bond formation occurs at a lateral position of around -1.5 nm. These covalent bonds contribute significantly to the resistive lateral force because they cause displacement of the bonded atoms from their original positions as the tip moves until the bonds break.<sup>6, 13</sup> As the applied normal load increases, the number of interfacial covalent bonds increases, resulting in higher lateral force. As the tip moves away from the step edge, the lateral force decreases gradually because the covalent bonds break one at a time. This gradual change of the lateral friction seems to be the characteristic feature of chemical contributions to friction; similar behavior is observed for the step-down friction measured in experiments (blue lines in Figure 2b) due to hydrogen bonding interactions of the OH groups at the step edge.<sup>6</sup>

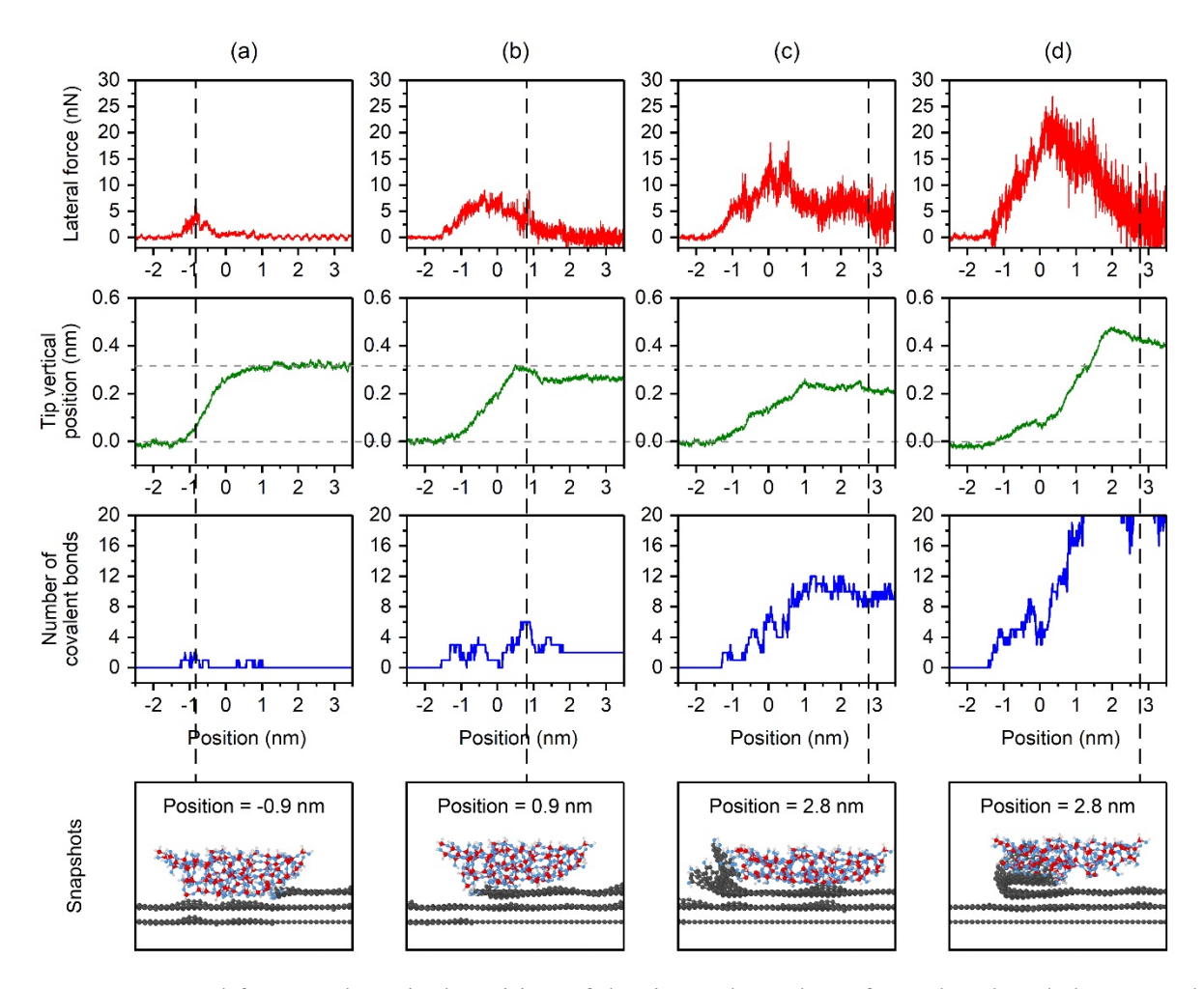


**Figure 4.** Lateral force and vertical position of the tip, and number of covalent bonds between the tip and the graphene step edge when a silica tip sliding over an exposed step edge at applied normal loads of (a) 5 nN, (b) 10 nN and (c) 15 nN. (d) A tip with three reactive sites at the bottom sliding over an exposed step edge at an applied normal load of 15 nN. Snapshots of the simulations at select lateral position for each case are presented as well.

Snapshots from the simulation are also shown in Figure 4 and Figure S4. When the applied normal load is 5 nN or 10 nN (Figures 4a and 4b), the number of the shear-induced covalent bonds is small, the peeling deformation of the upper terrace is negligible, and the deformed part of the upper terrace goes back to its original position after the covalent bonds break as the tip moves away from the step edge. When the applied normal load is 15 nN (Figure 4c and 4d), due to the large number of covalent bonds formed between the tip and the step edge, the entire upper terrace

is peeled upward when the tip is fully on the upper terrace (at 2.8 nm), and the covalent bonds do not break until the end of the simulation (at 3.5 nm).

Unlike the buckling case observed in experiments (Figure 2c), the tip vertical position during the peeling process does not significantly surpass the original vertical position of the upper terrace. In fact, the simulated tip vertical position on the upper terrace is slightly lower than the expected 0.34 nm (Figure 4c). As mentioned above, the recorded vertical position of the tip reflects the convolution of deformation or damage of the substrate and the bottom deformable part of the tip. As shown in Figure S5, the deformation of the top graphene layer during the sliding is the same for the lower and upper terrace regions. So, the recorded position being lower than the expected graphene layer thickness must be due to damage of the tip. In Figure S4c, it can be seen that the bottom part of the tip deforms due to chemical bonding with the step edge. Such deformation is much more severe when the load is increased (Figure S4a and S4b). The tip vertical position does not exceed the thickness of two layers (0.68 nm) even in the severe peeling case (Figure 4d). Note that, in all cases, the highest resistive lateral force appears before the vertical position reaches its maximum value. This may be another feature characteristic of tribochemical peeling deformation that could be used to determine if such deformation occurs or not during an experiment.

The fact that peeling is observed readily in our simulations but infrequently in experiments could be attributed to the size scale difference between the two. Specifically, the topographical corrugation of the graphene layer is determined by the competition between the graphene-substrate adhesion (which depends on the size of the graphene), the tip-graphene interaction (which depends on the tip-graphene contact area) and the intrinsic strength of graphene. When the graphene layer is much larger than the tip contact area, only the part of the graphene inside and around the contact area can be deformed, and deformation is limited by the bulk material far from the contact area. In

contrast, when the graphene layer and the contact area are comparable in size, the entire graphene layer can be easily deformed by the tip. In our simulations, the stacked graphene layers are only 4 nm wide and the width of the tip is 1.5 nm, and the sides of the graphene layers are not fixed (see Figure S3). As shown in Figure 4c, only about 10 covalent bonds between the step edge and the tip are enough to overcome the van der Waals interaction with the underlayer and peel up the 4 nm wide top layer. More severe deformation of the graphene layer is observed when the graphene step edge is more reactive and more covalent bonds can form between the silica tip and the step edge (see Figure 4d and Figure S6). In most AFM experiments, the step edges can be considered to be infinitely long compared to the contact area of the AFM tip. In this case, the peeling of the upper terrace layer due to tribochemical reactions is unlikely because the large van der Waals interactions of the large graphene sheet along the step edge would work against lifting of the upper terrace layer. Thus, only molecular functional groups at the step edge are likely deformed.<sup>13</sup> If significantly large number of covalent bonds were formed in AFM experiments to induce peeling, that may cause measurable changes of the tip surface and the step edge as well. However, no evidence of tip blunting or step edge alteration was found in our AFM experiments after hundreds of cycles of sliding (Figures S1 and S2). Tribochemical peeling may occur if the AFM tip slides at the corner site of the upper terrace where two steps meet and thus the graphene near the step edge can be considered to be very short, 8, 49 but this deformation mode is unlikely to be the dominant mechanism responsible for the high friction during the step-up sliding at typical straight step edges seen in most experimental conditions.

# 4 Conclusion

Based on the experimental and simulation results described in this paper, it can be concluded that an exposed graphene step edge exhibits much higher friction (or resistive lateral force) than the basal plane, even when there is no physical deformation or damage of the upper terrace layer at the step edge. The characteristic features of the lateral force and height profiles for three possible mechanisms causing high friction at the graphene step edge are summarized in Figure 6. When the upper terrace does not deform (Figure 6a), the lateral force (or lateral signal) exhibits the stick-slip behavior, i.e. a linear increase when the tip is stuck at the step followed by a sharp drop as it slips to the upper terrace. The slope of the linear increase is determined by the torsional spring of the AFM probe. The recorded height profile is very close to a step function in this case. When the upper terrace buckles due to physical stress (Figure 6b), the lateral force no longer increases linearly but still shows the sharp drop. In contrast to the no buckling case, the measured height is significantly above the vertical position of the pristine upper terrace since the tip is sliding on the buckled step. After passing the vertex of the buckled region, the tip experiences an assistive lateral force from the descending slope of the surface. Lastly, tribochemical covalent bond formation between the tip and the step edge can induce the peeling deformation of the upper terrace (Figure 6c). In this case, the lateral force increases and decreases gradually, and the maximum resistive lateral force occurs before the maximum position in the height profile. The height profile does not significantly exceed the vertical position of the upper terrace at any point.

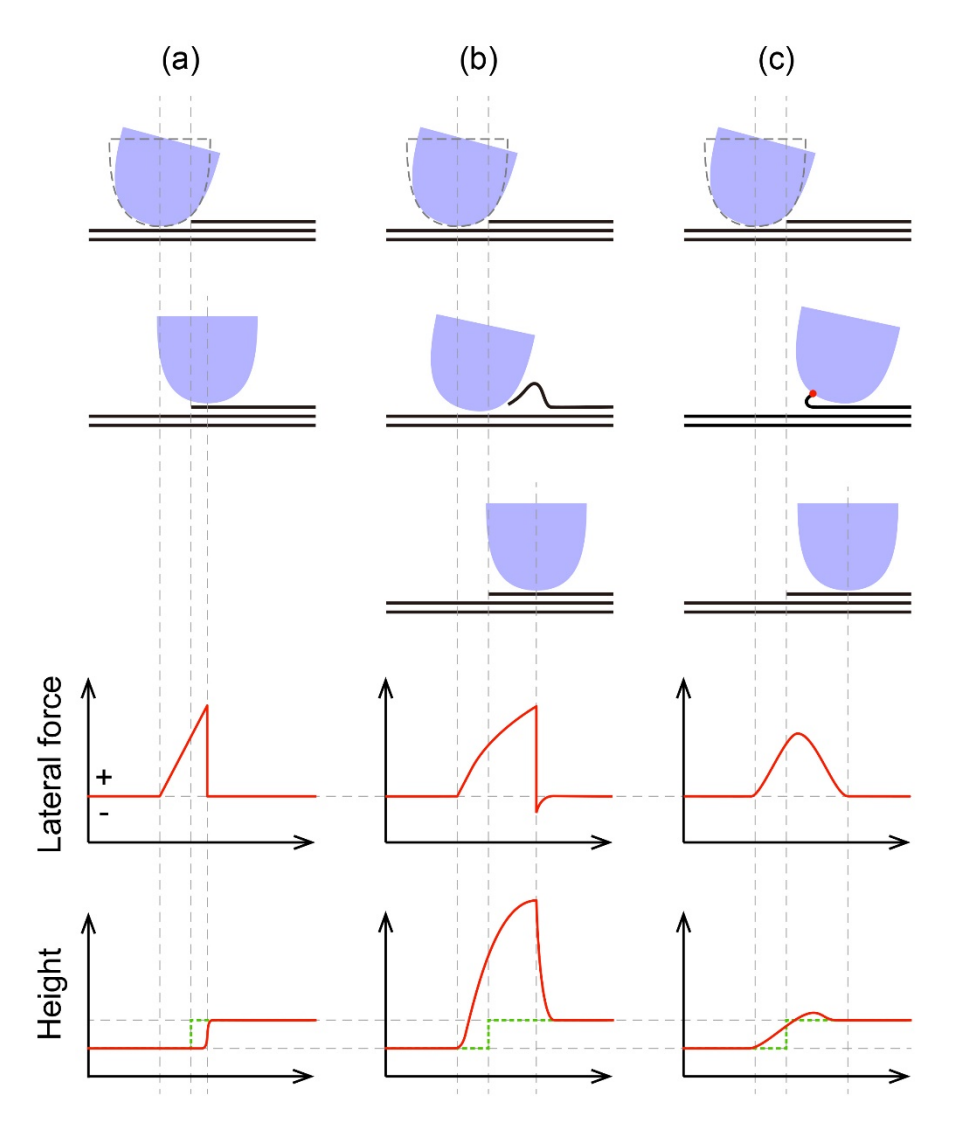


**Figure 5.** Schematics of a tip sliding across a single-layer graphene step edge from the lower terrace to the upper terrace for different friction mechanisms. (a) The tip exhibits stick-slip behavior and the step edge does not deform. (b) The upper terrace graphene layer is elastically buckled by interfacial shear and the tip slides over the buckled region leading to a height above the original upper terrace. (c) The upper terrace layer is peeled back due to shear-induced covalent bonds during the sliding motion because of the bonds, and the lateral force decreases gradually rather than sharply. The trends in lateral force and height characteristics of each mechanisms can be used as a reference to determine the origin of high friction measured at a step edge.

These features can be used to determine which mechanism is responsible for high friction measured with an AFM tip ascending a long and straight edge of a single layer graphene on the graphite basal plane. Our experimental results indicate that buckling of the graphene layer can

occur, particularly at higher loads, but this occurrence is rare. Also, the magnitude of friction

associated with buckling deformation is not necessarily larger than that of the stick-slip friction

without physical deformation of the layer. The experimental data do not exhibit the features

characteristic of tribochemical peeling deformation that are identified from MD simulations.

Comparing all experimental and computational results, it is concluded that the most likely

mechanism for high friction during the AFM tip step-up process at a graphene edge is stick-slip

behavior. Here we showed that this behavior is caused by both the step topography and the

chemical interactions between the functional groups at the step edge and the sliding tip, 6-7, 10, 13 as

opposed to the physical deformation of the graphene layer itself. These findings provide

fundamental understanding of the mechanisms underlying high friction observed when graphene

or graphite is used as a solid lubricant, and may be applicable to other 2D materials as well.

ASSOCIATED CONTENT

**Supporting Information** 

AFM force-distance curves on graphite basal plane; AFM lateral signal across a graphene step

edge; MD simulation model; snapshots of a tip sliding up a graphene step edge; vertical

deformation of the topmost graphene layer; analysis of the energy needed to peel and bend the

graphene layer.

**AUTHOR INFORMATION** 

**Corresponding Authors** 

\*Ashlie Martini. E-mail: amartini@ucmerced.edu

21

\*Seong H. Kim. E-mail: shkim@engr.psu.edu

#### **ORCID**

Zhe Chen: 0000-0002-5874-7196

Arash Khajeh: 0000-0002-9061-9370

Ashlie Martini: 0000-0003-2017-6081

Seong H. Kim: 0000-0002-8575-7269

#### **Notes**

The authors declare no competing financial interest.

#### ACKNOWLEDGMENTS

This work was supported by the National Science Foundation (Grant No. CMMI-1727571 and 1727356).

## REFERENCES

- (1) Tabor, D. Friction—the Present State of Our Understanding. J. Lubr. Technol. 1981, 103 (2), 169-179.
- (2) Lee, C.; Wei, X.; Li, Q.; Carpick, R.; Kysar, J. W.; Hone, J. Elastic and Frictional Properties of Graphene. *Phys. Status Solidi B* **2009**, *246* (11–12), 2562-2567.
- (3) Lee, C.; Li, Q.; Kalb, W.; Liu, X.-Z.; Berger, H.; Carpick, R. W.; Hone, J. Frictional Characteristics of Atomically Thin Sheets. *Science* **2010**, *328* (5974), 76-80.
- (4) Li, Q.; Lee, C.; Carpick, R. W.; Hone, J. Substrate Effect on Thickness-Dependent Friction on Graphene. *Phys. Status Solidi B* **2010**, *247* (11-12), 2909-2914.
- (5) Egberts, P.; Han, G. H.; Liu, X. Z.; Johnson, A. C.; Carpick, R. W. Frictional Behavior of Atomically Thin Sheets: Hexagonal-Shaped Graphene Islands Grown on Copper by Chemical Vapor Deposition. *ACS Nano* **2014**, *8* (5), 5010-5021.
- (6) Chen, Z.; Khajeh, A.; Martini, A.; Kim, S. H. Chemical and Physical Origins of Friction on Surfaces with Atomic Steps. *Sci. Adv.* **2019**, *5* (8), eaaw0513.
- (7) Chen, L.; Chen, Z.; Tang, X.; Yan, W.; Zhou, Z.; Qian, L.; Kim, S. H. Friction at Single-Layer Graphene Step Edges Due to Chemical and Topographic Interactions. *Carbon* **2019**, *154*, 67-73.
- (8) Vasić, B.; Matković, A.; Gajić, R.; Stanković, I. Wear Properties of Graphene Edges Probed by Atomic Force Microscopy Based Lateral Manipulation. *Carbon* **2016**, *107*, 723-732.
- (9) Qi, Y.; Liu, J.; Zhang, J.; Dong, Y.; Li, Q. Wear Resistance Limited by Step Edge Failure: The Rise and Fall of Graphene as an Atomically Thin Lubricating Material. *ACS Appl. Mater. Interfaces* **2017**, *9* (1), 1099-1106.

- (10) Chen, Z.; Kim, S. H. Measuring Nanoscale Friction at Graphene Step Edges. *Friction* **2020**, *8* (4), 802-811.
- (11) Hölscher, H.; Ebeling, D.; Schwarz, U. D. Friction at Atomic-Scale Surface Steps: Experiment and Theory. *Phys. Rev. Lett.* **2008**, *101* (24), 246105.
- (12) Ye, Z.; Martini, A. Atomic Friction at Exposed and Buried Graphite Step Edges: Experiments and Simulations. *Appl. Phys. Lett.* **2015**, *106* (23), 231603.
- (13) Chen, Z.; Khajeh, A.; Martini, A.; Kim, S. H. Identifying Physical and Chemical Contributions to Friction: A Comparative Study of Chemically Inert and Active Graphene Step Edges. *ACS Appl. Mater. Interfaces* **2020**, *12* (26), 30007-30015.
- (14) Dong, Y.; Liu, X. Z.; Egberts, P.; Ye, Z.; Carpick, R. W.; Martini, A. Correlation between Probe Shape and Atomic Friction Peaks at Graphite Step Edges. *Tribol. Lett.* **2013**, *50* (1), 49-57.
- (15) Hunley, D. P.; Flynn, T. J.; Dodson, T.; Sundararajan, A.; Boland, M. J.; Strachan, D. R. Friction, Adhesion, and Elasticity of Graphene Edges. *Phys. Rev. B* **2013**, *87* (3), 035417.
- (16) Lang, H.; Peng, Y.; Zeng, X. Effect of Interlayer Bonding Strength and Bending Stiffness on 2-Dimensional Materials' Frictional Properties at Atomic-Scale Steps. *Appl. Surf. Sci.* **2017**, *411*, 261-270.
- (17) Tripathi, M.; Awaja, F.; Bizao, R. A.; Signetti, S.; Iacob, E.; Paolicelli, G.; Valeri, S.; Dalton, A.; Pugno, N. M. Friction and Adhesion of Different Structural Defects of Graphene. *ACS Appl. Mater. Interfaces* **2018**, *10* (51), 44614-44623.
- (18) Yin, N.; Zhang, Z.; Zhang, J. Frictional Contact between the Diamond Tip and Graphene Step Edges. *Tribol. Lett.* **2019**, *67* (3), 75.
- (19) Qi, Y.; Liu, J.; Dong, Y.; Feng, X.-Q.; Li, Q. Impacts of Environments on Nanoscale Wear Behavior of Graphene: Edge Passivation Vs. Substrate Pinning. *Carbon* **2018**, *139*, 59-66.
- (20) Sader, J. E.; Larson, I.; Mulvaney, P.; White, L. R. Method for the Calibration of Atomic Force Microscope Cantilevers. *Rev. Sci. Instrum.* **1995**, *66* (7), 3789-3798.
- (21) Barnette, A. L.; Ohlhausen, J. A.; Dugger, M. T.; Kim, S. H. Humidity Effects on in Situ Vapor Phase Lubrication with N-Pentanol. *Tribol. Lett.* **2014**, *55* (1), 177-186.
- (22) Marino, M. J.; Hsiao, E.; Bradley, L. C.; Eryilmaz, O. L.; Erdemir, A.; Kim, S. H. Is Ultra-Low Friction Needed to Prevent Wear of Diamond-Like Carbon (DLC)? An Alcohol Vapor Lubrication Study for Stainless Steel/DLC Interface. *Tribol. Lett.* **2011**, *42* (3), 285.
- (23) Derjaguin, B. V.; Muller, V. M.; Toporov, Y. P. Effect of Contact Deformations on the Adhesion of Particles. *J. Colloid Interface Sci.* **1975,** *53* (2), 314-326.
- (24) Plimpton, S. Fast Parallel Algorithms for Short-Range Molecular Dynamics. *J. Comput. Phys.* **1995**, *117* (1), 1-19.
- (25) Alexander, S. Visualization and Analysis of Atomistic Simulation Data with Ovito—the Open Visualization Tool. *Modell. Simul. Mater. Sci. Eng.* **2010**, *18* (1), 015012.
- (26) Senftle, T. P.; Hong, S.; Islam, M. M.; Kylasa, S. B.; Zheng, Y.; Shin, Y. K.; Junkermeier, C.; Engel-Herbert, R.; Janik, M. J.; Aktulga, H. M.; Verstraelen, T.; Grama, A.; van Duin, A. C. T. The ReaxFF Reactive Force-Field: Development, Applications and Future Directions. *npj Comput. Mater.* **2016**, *2*, 15011.
- (27) Chipara, A. C.; Tsafack, T.; Owuor, P. S.; Yeon, J.; Junkermeier, C. E.; van Duin, A. C. T.; Bhowmick, S.; Asif, S. A. S.; Radhakrishnan, S.; Park, J. H.; Brunetto, G.; Kaipparettu, B. A.; Galvão, D. S.; Chipara, M.; Lou, J.; Tsang, H. H.; Dubey, M.; Vajtai, R.; Tiwary, C. S.; Ajayan, P. M. Underwater Adhesive Using Solid–Liquid Polymer Mixes. *Mater. Today Chem.* **2018**, *9*, 149-157.
- (28) Goverapet Srinivasan, S.; van Duin, A. C. T. Molecular-Dynamics-Based Study of the Collisions of Hyperthermal Atomic Oxygen with Graphene Using the ReaxFF Reactive Force Field. *J. Phys. Chem. A* **2011**, *115* (46), 13269-13280.
- (29) Chenoweth, K.; van Duin, A. C. T.; Goddard, W. A. ReaxFF Reactive Force Field for Molecular Dynamics Simulations of Hydrocarbon Oxidation. *J. Phys. Chem. A* **2008**, *112* (5), 1040-1053.

- (30) Chenoweth, K.; Cheung, S.; van Duin, A. C. T.; Goddard, W. A.; Kober, E. M. Simulations on the Thermal Decomposition of a Poly(Dimethylsiloxane) Polymer Using the ReaxFF Reactive Force Field. *J. Am. Chem. Soc.* **2005**, *127* (19), 7192-7202.
- (31) Jensen, B. D.; Wise, K. E.; Odegard, G. M. Simulation of the Elastic and Ultimate Tensile Properties of Diamond, Graphene, Carbon Nanotubes, and Amorphous Carbon Using a Revised ReaxFF Parametrization. *J. Phys. Chem. A* **2015**, *119* (37), 9710-9721.
- (32) Hou, Y.; Zhu, Y.; Liu, X.; Dai, Z.; Liu, L.; Wu, H.; Zhang, Z. Elastic–Plastic Properties of Graphene Engineered by Oxygen Functional Groups. *J. Phys. D: Appl. Phys.* **2017**, *50* (38), 385305.
- (33) Khajeh, A.; He, X.; Yeon, J.; Kim, S. H.; Martini, A. Mechanochemical Association Reaction of Interfacial Molecules Driven by Shear. *Langmuir* **2018**, *34* (21), 5971-5977.
- (34) Zandiatashbar, A.; Lee, G.-H.; An, S. J.; Lee, S.; Mathew, N.; Terrones, M.; Hayashi, T.; Picu, C. R.; Hone, J.; Koratkar, N. Effect of Defects on the Intrinsic Strength and Stiffness of Graphene. *Nat. Commun.* **2014**, *5* (1), 3186.
- (35) Walsh, T. R.; Wilson, M.; Sutton, A. P. Hydrolysis of the Amorphous Silica Surface. II. Calculation of Activation Barriers and Mechanisms. *J. Chem. Phys.* **2000**, *113* (20), 9191-9201.
- (36) Du, J.; Cormack, A. N. Molecular Dynamics Simulation of the Structure and Hydroxylation of Silica Glass Surfaces. *J. Am. Ceram. Soc.* **2005**, *88* (9), 2532-2539.
- (37) Yeon, J.; van Duin, A. C. T. ReaxFF Molecular Dynamics Simulations of Hydroxylation Kinetics for Amorphous and Nano-Silica Structure, and Its Relations with Atomic Strain Energy. *J. Phys. Chem. C* **2016**, *120* (1), 305-317.
- (38) Levita, G.; Restuccia, P.; Righi, M. C. Graphene and MoS2 Interacting with Water: A Comparison by Ab Initio Calculations. *Carbon* **2016**, *107*, 878-884.
- (39) Restuccia, P.; Ferrario, M.; Righi, M. C. Monitoring Water and Oxygen Splitting at Graphene Edges and Folds: Insights into the Lubricity of Graphitic Materials. *Carbon* **2020**, *156*, 93-103.
- (40) Jia, X.; Hofmann, M.; Meunier, V.; Sumpter, B. G.; Campos-Delgado, J.; Romo-Herrera, J. M.; Son, H.; Hsieh, Y.-P.; Reina, A.; Kong, J.; Terrones, M.; Dresselhaus, M. S. Controlled Formation of Sharp Zigzag and Armchair Edges in Graphitic Nanoribbons. *Science* **2009**, *323* (5922), 1701.
- (41) Asay, D. B.; Hsiao, E.; Kim, S. H. Corrected Direct Force Balance Method for Atomic Force Microscopy Lateral Force Calibration. *Rev. Sci. Instrum.* **2009**, *80* (6), 066101.
- (42) Green, C. P.; Lioe, H.; Cleveland, J. P.; Proksch, R.; Mulvaney, P.; Sader, J. E. Normal and Torsional Spring Constants of Atomic Force Microscope Cantilevers. *Rev. Sci. Instrum.* **2004**, *75* (6), 1988-1996.
- (43) Garvey, M.; Weinert, M.; Tysoe, W. T. On the Pressure Dependence of Shear Strengths in Sliding, Boundary-Layer Friction. *Tribol. Lett.* **2011**, *44* (1), 67.
- (44) Martini, A.; Eder, J. S.; Dörr, N. Tribochemistry: A Review of Reactive Molecular Dynamics Simulations. *Lubricants* **2020**, *8* (4), 44.
- (45) Gosvami, N. N.; Bares, J. A.; Mangolini, F.; Konicek, A. R.; Yablon, D. G.; Carpick, R. W. Mechanisms of Antiwear Tribofilm Growth Revealed in Situ by Single-Asperity Sliding Contacts. *Science* **2015**, *348* (6230), 102.
- (46) Zhang, J.; Ewen, J. P.; Ueda, M.; Wong, J. S. S.; Spikes, H. A. Mechanochemistry of Zinc Dialkyldithiophosphate on Steel Surfaces under Elastohydrodynamic Lubrication Conditions. *ACS Appl. Mater. Interfaces* **2020**, *12* (5), 6662-6676.
- (47) He, X.; Kim, S. H. Surface Chemistry Dependence of Mechanochemical Reaction of Adsorbed Molecules—an Experimental Study on Tribopolymerization of A-Pinene on Metal, Metal Oxide, and Carbon Surfaces. *Langmuir* **2018**, *34* (7), 2432-2440.
- (48) Chen, Z.; Vazirisereshk, M. R.; Khajeh, A.; Martini, A.; Kim, S. H. Effect of Atomic Corrugation on Adhesion and Friction: A Model Study with Graphene Step Edges. *J. Phys. Chem. Lett.* **2019**, *10* (21), 6455-6461.

(49) Schniepp, H. C.; Kudin, K. N.; Li, J.-L.; Prud'homme, R. K.; Car, R.; Saville, D. A.; Aksay, I. A. Bending Properties of Single Functionalized Graphene Sheets Probed by Atomic Force Microscopy. *ACS Nano* **2008**, *2* (12), 2577-2584.